Magnetic Anomaly Detection using Noise-Optimized Orthonormalized Functions on dual magnetometric sensor signals

Timothée Roignant, Nicolas Le Josse, Abdel Boudraa, Jean-Jacques Szkolnik, Paul Penven, Hugues Henocq

Magnetic Anomaly Detection using Noise-Optimized Orthonormalized Functions on dual magnetometric sensor signals

Timothée Roignant*†, Nicolas Le Josse†, Abdel Boudraa*, Jean-Jacques Szkolnik*,
Paul Penven† and Hugues Henocq‡

*Ecole Navale/Arts & Metiers Institute of Technology, IRENav, BCRM Brest, CC 600, 29 240 Brest, France
†Thales - Brest, France
‡DGA-TN - 29 240 Brest, France

***Abstract*—The performances of classic matched filter approaches for magnetic dipole detection are limited due to the correlated nature of the environmental magnetic noise. For this reason, several studies have proposed background noise optimization of the classic matched filter, but only for single-sensor applications. In this study, we extend the noise-optimized matched filter for the detection of a ferromagnetic object to dual-sensor scalar magnetometric applications, and we provide the associated formal development. The noise-optimized matched filter is built by whitening the classic orthonormalized basis functions of the original matched filter by the sampled background noise covariance matrix, according to the minimum variance distortionless response criterion. The receiver operating characteristic curves show a +2 dB processing gain between the original matched filter and the noise-optimized one when they are applied to a ferromagnetic object signal placed in a colored noise environment. Moreover, for dual-sensor signals, an additional array gain of +3 dB is observed in comparison with a single magnetic sensor, meaning that the proposed method has a total gain of +5dB compared to the original matched filter applied to a single-sensor signal. These results are encouraging for the use of magnetometric array processing techniques in the future.**

***Index Terms*—Magnetic Anomaly Detection, Matched Filter, Orthonormalized Basis Functions, Minimum Variance Distortionless Response, Array processing**

I. Introduction

Magnetic anomaly detection (MAD) is a passive complementary method to the use of SONAR systems for detecting ferromagnetic objects such as metallic wastes, mines, unexploded ordnances (UXO), wrecks, ships, pipelines, or submarines [1], [2]. The object generates a magnetic field, resulting in a local anomaly in the Earth's magnetic field that can be measured as a time-varying signal by a magnetic sensor that moves in the vicinity of the object [2]. However, the magnetometer also senses the different magnetic fields of all the magnetic sources in the environment (such as geological sources, oceanic motion's magnetic fields, and geomagnetic fluctuations [3]). Hence, it is necessary to process the measured signal to detect the object signature that is generally drowned in the background noise. The most common detection method is to decompose the signal of the object into a set of orthonormalized basis functions (OBF) [4]. OBF performs well under Gaussian white background noise, but their performances degrade under colored noise with a $1/f^{\alpha}$ power spectral density (PSD), which is a good representation of the common environmental magnetic background noise [5]. Several methods have been proposed in the literature to extend the use of the OBF matched filter to colored background noise, but to the best of our knowledge, these methods have only been applied to single sensor detection systems [5], [6], [7], [8], [9]. However, recent advances regarding sensor miniaturization have enabled the use of embedded magnetometric arrays for MAD systems [10]. Therefore, it is crucial to have efficient array processing techniques. The present work's main contribution is to apply the Minimum Variance Distortionless Response (MVDR) criterion [11] to the OBF matched filter in order to build a noise-optimized matched filter and test its ability to detect ferromagnetic's signatures under colored noise environments in dual-sensor magnetometric signals.

This work was partially funded by the French Defense Innovation Agency (Grant No.2021857)

II. Dual-sensor detection procedure

Generally, the sensor-to-object distance R is large enough (more than 3 times the largest dimension of the object) to consider the object as a magnetostatic dipole [4]. The magnetic field $\mathbf{B}$ of the object with a magnetic moment $\mathbf{M}$ at a distance $R = \|\mathbf{r}\|$ can be expressed as:

$$\mathbf{B} = \frac{\mu_0}{4\pi R^5}\left[3(\mathbf{M}\cdot\mathbf{r})\mathbf{r} - R^2\mathbf{M}\right] \tag{1}$$

($\mu_0 = 4\pi \times 10^{-7}$ H/m being the permeability of the free space). For scalar magnetometers, the measured object signal S can be approximated by the projection of the object's magnetic field $\mathbf{B}$ onto the local Earth's magnetic field $\mathbf{T}$ [4]:

$$S = \frac{\mathbf{B}\cdot\mathbf{T}}{\|\mathbf{T}\|} \tag{2}$$

As the sensor also measures the ambient magnetic noise, the raw signal X is expressed as $X(n) = S(n) + N(n)$, where N is the additive background noise and n is a given temporal sample of the signal measured at the sampling frequency f_s.

The Signal to Noise Ratio (SNR, in decibels) is then defined as in [12], [8]:

$$\text{SNR} = 20\log_{10}\frac{\max(|S|)}{\sqrt{\frac{1}{L}\sum_{i=1}^{L}\left(N(i)-\overline{N}\right)^2}} \quad \text{dB} \qquad (3)$$

where S is the original anomaly of finite length L and $\overline{N}$ the mean value of the background noise N. An example of an object's magnetic anomaly signal polluted by a colored background noise is given in fig.1. The colored noise samples are generated by manipulating the Fast Fourier Transform (FFT) of a random white noise so that the amplitudes get proportional to $1/\sqrt{f^{\alpha}}$ before applying the inverse FFT, with α being the power law coefficient of the PSD. The typical α value of the magnetic environmental noise has been estimated in the $[0;2]$ range [5]. Hence, the background noise displayed on fig.1 was generated with an arbitrary value of $\alpha = 1$, which corresponds to a pink noise.

Fig.2 describes the geometry related to the measurement of the object's magnetic anomaly by the magnetic sensors. The sensor platform moves along a straight line represented by the x-axis in the vicinity of the static object positioned at a point defined by $(x_O; y_O; z_O)$. The x-axis is laterally shifted from the object by a distance s and the platform velocity V_0 and relative altitude h are both constant. Under these assumptions: $R^2 = (V_0 t - x_O)^2 + y_O^2 + z_O^2$, with t the time. The point on the x-axis reached at a time t_{CPA} such as $V_0 t_{CPA} = x_O$ is called the Closest Point of Approach (CPA). At the CPA, R reaches its minimum R_0 given by $R_0^2 = s^2 + h^2$. It is then possible to express R as a function of the CPA-normalized distance w, such as: $R^2 = R_0^2(1 + w^2)$, with:

$$w = R_0^{-1} V_0 (t - t_{CPA}) \qquad (4)$$

Applying the same reasoning to the second sensor gives: $R_2^2 = R_{00}^2(1 + w_2^2)$, with w_2 being the distance ratio between the second sensor-to-object distance R_2 and the second sensor-to-CPA distance R_{00}. As both sensors are embedded on the same platform, it is more convenient to consider a normalized

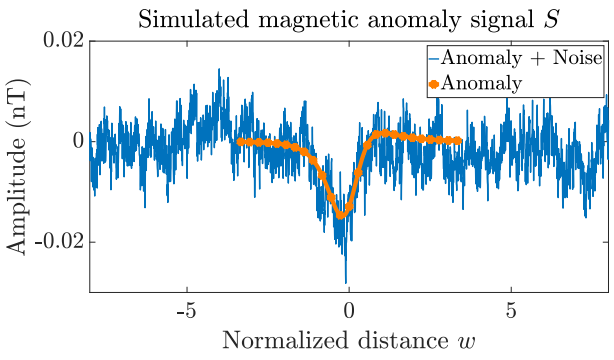

Fig. 1: Example of a magnetic anomaly signal S polluted by a zero-mean Gaussian pink noise N ($f_s = 10$Hz, $\alpha = 1$). The SNR at this sampling frequency is -9 dB.

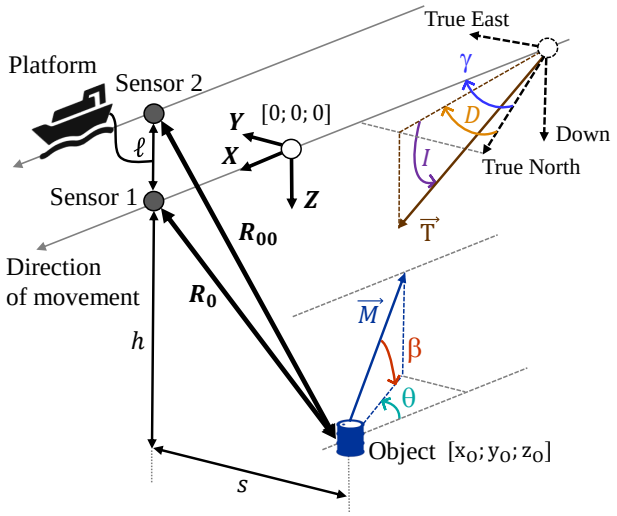

Fig. 2: Representation the object's magnetic anomaly signal measurement by an embedded dual-sensor system that moves along a straight line of γ heading. M is the magnetic moment of the object, with θ being its magnetic declination and β being its magnetic inclination. T is the local geomagnetic field, with D being the geomagnetic declination and I being the geomagnetic inclination (Reworked from [4]).

distance between the sensor platform and its CPA rather than normalized distances between each sensor and their respective CPA. This is done by considering the first sensor as the reference sensor, such as $w_2 = R_{00}^{-1} V_0 (t - t_{CPA}) = d \times w$, where d can be considered as an array baseline coefficient defined as in [4]:

$$d = \sqrt{\left(\frac{R_0^2}{R_{00}^2}\right)} = \sqrt{\left(\frac{s^2 + h^2}{s^2 + (h + \ell)^2}\right)} \qquad (5)$$

Combining (4), (5), (1) and (2) leads to express the dual-sensor magnetic anomaly $[S]$ of the object as a linear combination of several functions $F(w)$ such as: $[S] = [\lambda][F(w)]$, where:

$$\begin{bmatrix} S_1 \\ S_2 \end{bmatrix} = \begin{bmatrix} \lambda_1 & \lambda_2 & \lambda_3 & 0 & 0 & 0 \\ 0 & 0 & 0 & \lambda_4 & \lambda_5 & \lambda_6 \end{bmatrix} \begin{bmatrix} F_1(w) \\ F_2(w) \\ F_3(w) \\ F_4(w) \\ F_5(w) \\ F_6(w) \end{bmatrix} \qquad (6)$$

with $F_n(w)$ defined as in [4]:

$$\begin{aligned} F_1(w) &= k_1\left((1+w^2)^{-5/2} + k_0 w^2 (1+w^2)^{-5/2}\right) \\ F_2(w) &= k_2 w (1+w^2)^{-5/2} \quad F_3(w) = k_3 w^2 (1+w^2)^{-5/2} \\ F_4(w) &= k_1\left(d^3(1+(dw)^2)^{-5/2} + k_0 d^5 w^2 (1+(dw)^2)^{-5/2}\right) \\ F_5(w) &= k_2 d^4 w (1+(dw)^2)^{-5/2} \\ F_6(w) &= k_3 d^5 w^2 (1+(dw)^2)^{-5/2} \end{aligned} \qquad (7)$$

where $F_n(w)$ is the orthonormalized basis function (OBF) number n (displayed in fig.3 for the first sensor signal, spanning $n = 1, 2, 3$) and λ_n is the corresponding OBF coefficient. The OBF in (7) are expressed with the orthonormalization coefficients k_n resulting from the Gram-Schmidt procedure used to gain better detection properties from the original basis functions, called "Anderson functions", and developed in the late 1940's to express the magnetic field of a ferromagnetic object [3]. The k_n coefficients are given by:

$$k_0 = -\frac{5}{3};\ k_1 = \sqrt{\frac{24}{5\pi}};\ k_2 = \sqrt{\frac{128}{5\pi}};\ k_3 = \sqrt{\frac{128}{3\pi}} \tag{8}$$

By developing (1) and (2) with respect to (4), we calculated the dual-sensor OBF coefficients λ that are relevant for the scenario given in fig.2 and used in (6). They are given by:

$$\begin{aligned}
\lambda_1 &= \frac{M_0\mu_0}{4\pi {R_0}^3}\frac{\begin{array}{r}((a_3-1)m_Y + a_4 m_Z)e_Y\\ +(a_4 m_Y + (a_5-1)m_Z)e_Z - m_X e_X\end{array}}{k_1}\\
\lambda_2 &= \frac{M_0\mu_0}{4\pi {R_0}^3}\frac{(a_1 m_Y + a_2 m_Z)e_X + a_1 m_X e_Y + a_2 m_X e_Z}{k_2}\\
\lambda_3 &= \frac{M_0\mu_0}{4\pi {R_0}^3}\frac{\begin{array}{r}2m_X e_X - m_Y e_Y - m_Z e_Z\\ -k_0\big[\big((a_3-1)m_Y + a_4 m_Z\big)e_Y\\ +\big(a_4 m_Y + (a_5-1)m_Z\big)e_Z - m_X e_X\big]\end{array}}{k_3}\\
\lambda_4 &= \frac{M_0\mu_0}{4\pi {R_0}^3}\frac{\begin{array}{r}\big((b_3-1)m_Y + b_4 m_Z\big)e_Y\\ \big(b_4 m_Y + (b_5-1)m_Z\big)e_Z - m_X e_X\end{array}}{k_1}\\
\lambda_5 &= \frac{M_0\mu_0}{4\pi {R_0}^3}\frac{\big(b_1 m_Y + b_2 m_Z\big)e_X + b_1 m_X e_Y + b_2 m_X e_Z}{k_2}\\
\lambda_6 &= \frac{M_0\mu_0}{4\pi {R_0}^3}\frac{\begin{array}{r}2m_X e_X - m_Y e_Y - m_Z e_Z\\ -k_0\big[\big((b_3-1)m_Y + b_4 m_Z\big)e_Y\\ +\big(b_4 m_Y + (b_5-1)m_Z\big)e_Z - m_X e_X\big]\end{array}}{k_3}
\end{aligned} \tag{9}$$

with the following geometrical components:

$$\begin{aligned}
&a_1 = 3sR_0^{-1} \quad a_2 = 3hR_0^{-1} \quad a_3 = 3s^2R_0^{-2} \quad a_4 = 3shR_0^{-2}\\
&a_5 = 3h^2R_0^{-2} \quad b_1 = 3sR_{00}^{-1} \quad b_2 = 3(h+\ell)R_{00}^{-1}\\
&b_3 = 3s^2R_{00}^{-2} \quad b_4 = 3s(h+\ell)R_{00}^{-2} \quad b_5 = 3(h+\ell)^2R_{00}^{-2}
\end{aligned} \tag{10}$$

and the following magnetic parameters:

$$\begin{aligned}
&\mathbf{M} = \begin{bmatrix}M_X\\M_Y\\M_Z\end{bmatrix} = M_0\begin{bmatrix}m_X\\m_Y\\m_Z\end{bmatrix} \text{ and } \mathbf{T} = \begin{bmatrix}T_X\\T_Y\\T_Z\end{bmatrix} = \|\mathbf{T}\|\begin{bmatrix}e_X\\e_Y\\e_Z\end{bmatrix}\\
&m_X = \cos(\theta)\left(\cos(\beta) + \sin(\beta)\right) - \sin(\theta)\\
&m_Y = \sin(\theta)\cos(\beta) + \cos(\theta) + \sin(\theta)\sin(\beta)\\
&m_Z = \cos(\beta) - \sin(\beta)\\
&e_X = \cos(D+\gamma)\sin(I) - \sin(D+\gamma) + \cos(D+\gamma)\cos(I)\\
&e_Y = \sin(D+\gamma)\sin(I) + \cos(D+\gamma) + \sin(D+\gamma)\cos(I)\\
&e_Z = \sin(I) - \cos(I)
\end{aligned} \tag{11}$$

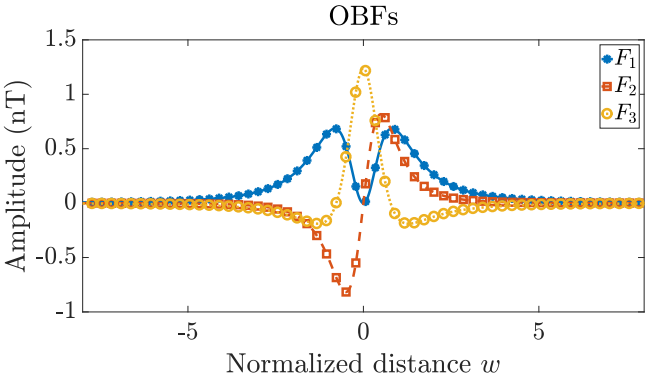

Fig. 3: Typical set of OBF for a single sensor with a straight-line flight path.

In single sensor applications, since R_0 is unknown a priori, the detection procedure is made through multi-channel filters, each channel corresponding to an estimated value of R_0 [4]. For dual-sensor applications, the multi-channel filters must be adapted to span through different combinations of s and h values for a selected value of R_0. Then, the value of the array baseline coefficient d will be automatically adapted through each channel according to both ℓ and the selected value of assumed $R_0 = \sqrt{s^2 + h^2}$. Moreover, in order to effectively detect the object's magnetic anomaly in the measured signal, the filtering procedure is made over a sliding window of δ half-width, corresponding to the length of the overlap between the OBF and the object's magnetic anomaly. Under these considerations, the detection of a time-discrete measured signal S is made when the total energy E of the decomposed raw signal in the basis of the OBF at a certain point m of signal processing exceeds a certain threshold. The total energy is given by the sum of the energy of the OBF coefficients, with Δw the length of spatial sampling normalized to the CPA-distance, such as in [4]:

$$E_1(m) = \sum_{n=1}^{3}\left|\sum_{i=-\delta}^{+\delta} F_n(w_i)S_1(w_{m+i})\ \ \Delta w\right|^2 \tag{12}$$

where $\Delta w = w_{i+1} - w_i$

Results of this filtering operation on the same anomaly as depicted in fig.1 under both Gaussian white and pink noises are given in fig.4. It can be seen in fig.4a that this operation is optimal under white noise conditions. However, under pink noise conditions, as illustrated in fig.4b, peaks of normalized energy arise outside the $[-w; w]$ range, which indicates the presence of false alarms for thresholds inferior to 50% of the maximum normalized energy in this example.

III. Noise-optimized matched filter

The output Y of a noise-optimized detector can be expressed as [11]:

$$Y = W^H\ [X] = W^H\ [F] + W^H\ [N] \tag{13}$$

with W the optimal weight vector for the set of measurements on the whole array $[X]$ and the object's magnetic anomaly signals $[S]$ (which is unknown), expressed by the OBF $[F]$ as defined in relation (7). The aim is to find the optimal vector W that maximizes the SNR in the presence of the signal of interest by minimizing the variance of Y in the presence of noise under the constraint of no distortion of the signal of interest [11]. Therefore, W must verify the two following conditions given by:

$$\begin{cases} W^H\ [F] = 1 \\ \min\left(W^H\ [N]\right) \end{cases} \tag{14}$$

As demonstrated in [9]: $\min\left(W^H[N]\right) = \min\left(W^H \Gamma W\right)$, where Γ is the covariance matrix of the noise. This double constraint can be expressed as a Lagrange optimization problem [9], [11]. The goal is to find the minima of the Ψ function defined as

$$\Psi(W,\ \xi) = \min\left(W^H \Gamma W\right) + \xi\left(W^H F - 1\right) \tag{15}$$

with ξ being the Lagrange multiplier. By solving $\nabla_{W^H}\Psi = 0$ as in [9], W becomes:

$$W = \frac{\Gamma^{-1}\ F}{F^H\ \Gamma^{-1}\ F} \tag{16}$$

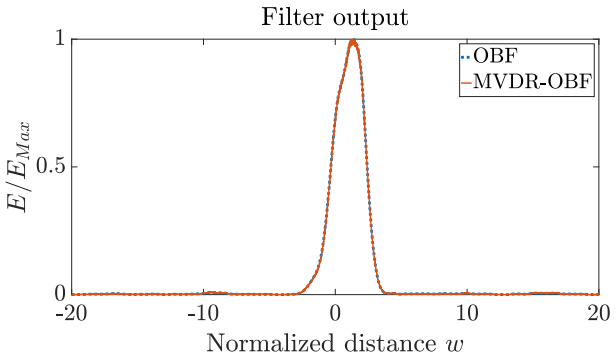

(a) White noise case ($\alpha = 0$)

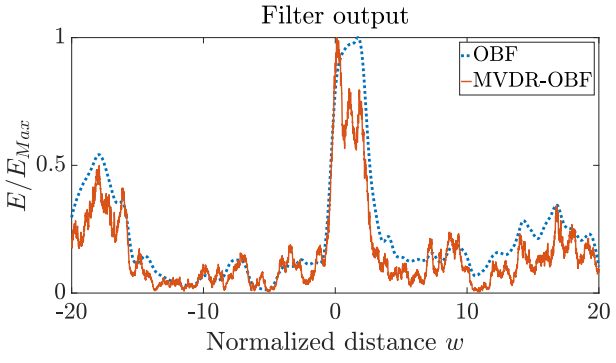

(b) Pink noise case ($\alpha = 1$)

Fig. 4: Output of the filtering procedure for the same magnetic anomaly as shown in fig.1. The original anomaly is polluted by zero-mean Gaussian noise (SNR= -9dB, $\delta = 2w$).

with $[F^H\Gamma^{-1}F]^{-1}$ being the scaling factor or normalizing coefficient for unity gain and W being the array weight for the minimum variance distortionless response [11]. It is now possible to process the array signal $[S]$ with the noise-covariance-weighted OBF W in the same manner as for (12):

$$[E(m)] = \left| \sum_{i=-\delta}^{+\delta} W(w_i)[S(w_{m+i})]\ \ \Delta w \right|^2 \tag{17}$$

with: $\Delta w = w_{i+1} - w_i$

This implies that the computation of Γ is made through the same sliding window of δ half-width as in (17). For a signal of length L, the mean covariance of the noise can be estimated through a sliding window as follows:

$$\Gamma = \frac{2\delta}{L} \sum_{i=0}^{L/2\delta} N(2\delta i + 1 : 2\delta i + 2\delta)\ N(2\delta i + 1 : 2\delta i + 2\delta)^H \tag{18}$$

where the subscript H denotes the Hermitian transpose. Results of this filtering applied to the same anomaly as depicted in fig.1 under both Gaussian white and pink noises are given in fig.4. Under white noise conditions, fig.4a shows no improvement of the MVDR-OBF filter over the OBF filter. The two filters performs similarly because the OBF filter is already the optimal one under white noise conditions, as the covariance matrix of a white noise is a diagonal matrix with its diagonal elements being the power of the noise [7], [9]. However, for colored noises, fig.4b shows that noise-covariance whitening damps the amplitude of false alarms and narrows the peaks of normalized energy.

It is worth noticing that for single-sensor signals, this operation whitens the background noise and simultaneously performs the energy computation. However, for dual-sensor signals, this operation also denoise the original signal, as the diagonal element $\Gamma(m,m)$ is the power of the noise sample m and $\Gamma(m,p)$ is the cross-correlation of samples m and p on the sensors that tend to be mitigated during the whitening operation.

IV. Results

The detection strategy can be described as a binary decision problem:

$$\begin{cases} H_0 : X = N \\ H_1 : X = S + N \end{cases} \tag{19}$$

where H_0 and H_1 are respectively the object signal absence and presence hypothesis. The output of the detector can then give four outcomes: either the sample is correctly classified under the H_1 hypothesis (true positive case "TP") or incorrectly classified (false negative case "FN"), or either the sample is correctly classified under the H_0 hypothesis (true negative case "TN") or incorrectly classified (false negative case "FP").

To compare the performances of both OBF and MVDR-OBF matched filters, the probability of detection P_D and the probability of false alarms P_{FA} for both matched filters applied to a dataset of magnetic anomaly signals polluted by colored noises are computed. These two quantities are given by:

$$P_D = \frac{TPs}{TPs + FNs} \quad P_{FA} = \frac{FPs}{FPs + TNs} \tag{20}$$

The associated Receiver Operating Characteristics (ROC) curves are shown in fig.5. To see the relative gain between the methods without bias, the ROC curves are computed with a constant value of $\alpha = 1$ and an arbitrary value of SNR = "SNR_0", which we consider to be an operating functioning point for application in the marine environment. The dataset used to compute the probabilities comprise 8000 signals, which enables a sufficient number of snapshots while limiting computational costs. For dual-sensor signals, we chose an arbitrary constant value of ℓ =10, while keeping the half-width window of $\delta = 2w$ for the detection procedure given in (18). The results displayed in fig.5 show an improvement of +2 dB between the original OBF method and the MVDR-OBF one. Moreover, adding a second sensor improves the processing gain by approximately +3dB in the MVDR-OBF case. This is due to the fact that a second sensor doubles the number of samples for the noise covariance estimation, which improves the noise adaptation. This results in an overall improvement of +5dB between the single-sensor OBF case and the dual-sensor noise-optimized one. Regarding the inverse cubic law of decay of the object's dipolar magnetic field given in equation (1) and the SNR definition given in relation (3), this improvement in gain of +5dB is equivalent to a 21% improvement on the range of detection. These results show the interest in embedded magnetometric arrays for magnetic anomaly detection.

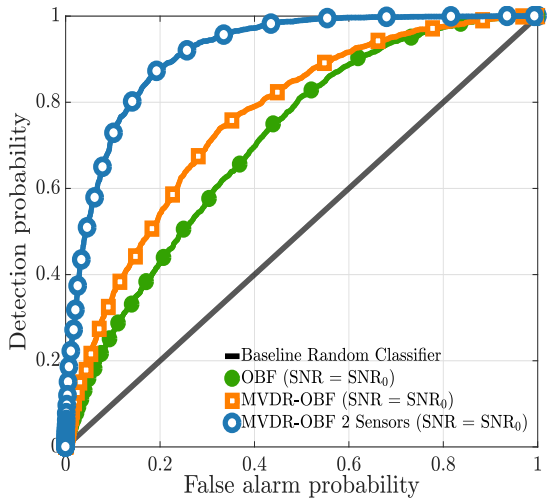

Fig. 5: ROC curves for magnetic anomalies polluted by zero-mean Gaussian pink noise. Single-sensor and dual-sensor cases are displayed, both with (MVDR-OBF) and without (OBF) noise-covariance whitening.

V. Conclusion

In this work, an extension of the MVDR-noise-optimized matched filter to dual magnetometric sensor signals is proposed. To our knowledge, this extension has not been proposed yet. For ferromagnetic object signals polluted by colored noise, the proposed method shows an improvement in detection rate according to array processing theory. This approach enables background noise reduction using a second sensor without having to perform gradiometric differentiation, which gives a better range of detection since gradiometric signals decrease more rapidly than magnetometric signals [12]. For future work, we plan to test the method on real signals in order to gain a better insight into its performance under real-noise conditions. Also, noise coherence tests should be run on the sensors to determine the number of optimal sensors and their spacing to be set on the array for a given detection scenario. Finally, a comparison between this method and the traditional gradiometric OBF one could help us determine the most appropriate use case for each of the two methods.

References

[1] J. Lenz and S. Edelstein, "Magnetic sensors and their applications," *IEEE Sensors Journal*, vol. 6, no. 3, pp. 631–649, 2006.

[2] J. J. Holmes, *Exploitation of a ship's magnetic field signatures*, M. . Claypool, Ed. San Mateo, CA, USA: Springer Nature, 2006.

[3] R. Otnes, "Static magnetic dipole detection using vector linear prediction, anderson functions, and block-based adaptive processing," in *OCEANS 2007 - Europe*, Aberdeen, UK, 2007, pp. 1–6.

[4] B. Ginzburg, L. Frumkis, and B.-Z. Kaplan, "Processing of magnetic scalar gradiometer signals using orthonormalized functions," *Sensors and Actuators A: Physical*, vol. 102, pp. 67–75, 2002.

[5] A. Sheinker, A. Shkalim, N. Salomonski, B. Ginzburg, L. Frumkis, and B.-Z. Kaplan, "Processing of a scalar magnetometer signal contaminated by $1/f^{\alpha}$ noise," *Sensors and Actuators A: Physical*, vol. 138, no. 1, pp. 105–111, 2007.

[6] X. Zheng, Q. Xu, Q. Li, and X. Hu, "An orthonormalized basis function based narrowband filtering algorithm for magnetic anomaly detection," in *2016 9th International Congress on Image and Signal Processing, BioMedical Engineering and Informatics (CISP-BMEI)*, Datong, China, 2016, pp. 119–123.

[7] S. Zozor, L.-L. Rouve, G. Cauffet, J.-L. Coulomb, and H. Henocq, "Compared performances of MF-based and locally optimal-based magnetic anomaly detection," in *2010 18th European Signal Processing Conference*, Aalborg, Denmark, 2010, pp. 149–153.

[8] C. Wan, M. Pan, Q. Zhang, D. Chen, H. Pang, and X. Zhu, "Performance improvement of magnetic anomaly detector using Karhunen–Loeve expansion," *IET Science, Measurement & Technology*, vol. 11, no. 5, pp. 600–606, 2017.

[9] M. K. Hu, C. P. Du, H. D. Wang, M. Y. Xia, X. Peng, and H. Guo, "Optimized basis functions under gaussian color noise for magnetic target signal detection," *IEEE Geoscience and Remote Sensing Letters*, vol. 18, no. 5, pp. 806–810, 2021.

[10] J. S. Bennett, B. E. Vyhnalek, H. Greenall, E. M. Bridge, F. Gotardo, S. Forstner, G. I. Harris, F. A. Miranda, and W. P. Bowen, "Precision magnetometers for aerospace applications: A review," *Sensors*, vol. 21, 5568, 2021.

[11] H. Van Trees, *Optimum array processing: part IV of detection, estimation, and modulation theory*. Wiley, 2002.

[12] L. Fan, C. Kang, H. Hu, X. Zhang, J. Liu, X. Liu, and H. Wang, "Gradient signals analysis of scalar magnetic anomaly using orthonormal basis functions," *Measurement Science and Technology*, vol. 31, no. 11, p. 115105, 2020.